Supplementary Information for
Improved performance and stability in quantum dot solar cells through band alignment engineering

Chia-Hao M. Chuang[1], Patrick R. Brown[2], Vladimir Bulović[3] & Moungi G. Bawendi[4*]

[1]Department of Materials Science and Engineering,
[2]Department of Physics,
[3]Department of Electrical Engineering and Computer Science,
[4]Department of Chemistry, Massachusetts Institute of Technology, Cambridge, Massachusetts, 02139, United States.
*email: mgb@mit.edu

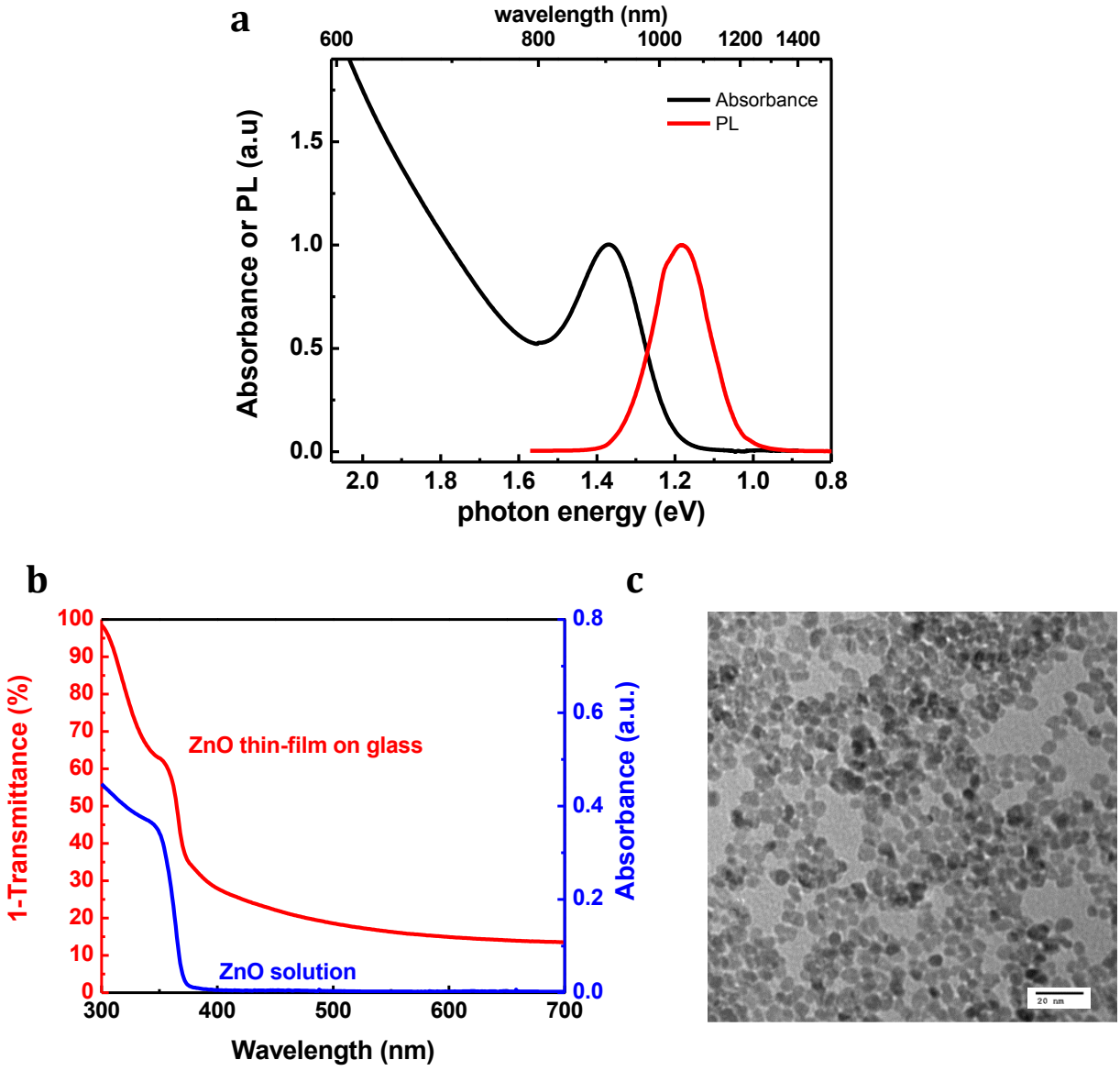

Figure S1 | Materials characterization. a, Absorption and photoluminescence spectra of PbS QDs in octane solution. **b,** Absorption spectra of ZnO nanocrystal solution and ZnO thin film on glass substrate. The absorption onset at wavelength λ~370nm corresponds to a bandgap of ~3.35eV. The background at longer wavelengths in the thin film absorption spectrum is due to light scattering and reflection. **c,** TEM image of ZnO nanocrystals (scale bar: 20nm).

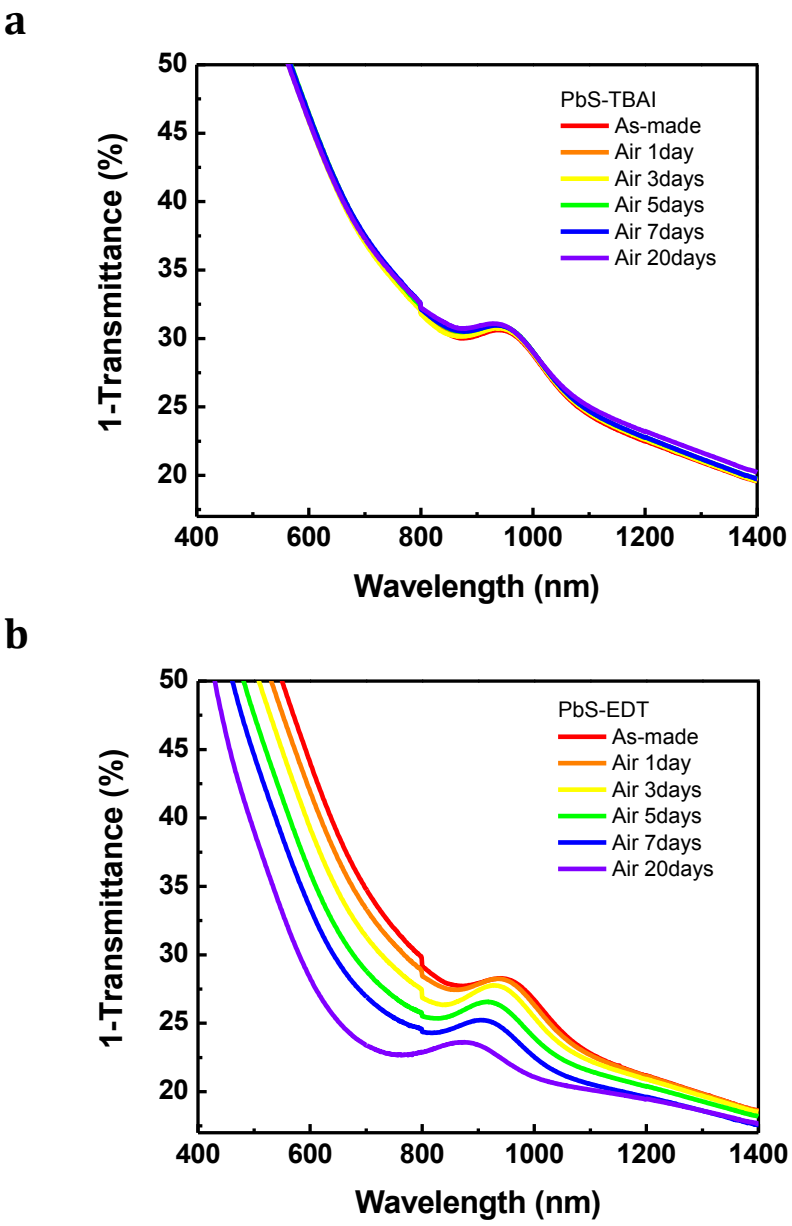

Figure S2 | Evolution of absorption spectra of PbS thin films (2 layers) with air storage time. a, The absorption spectra of the PbS-TBAI film shows no apparent change, indicating good stability. **b,** The absorption spectra of the PbS-EDT film shows a monotonic decrease in intensity and blue shift with air storage time as a result of oxidation. The discontinuity at wavelength λ=800nm is an artifact resulting from detector changeover.

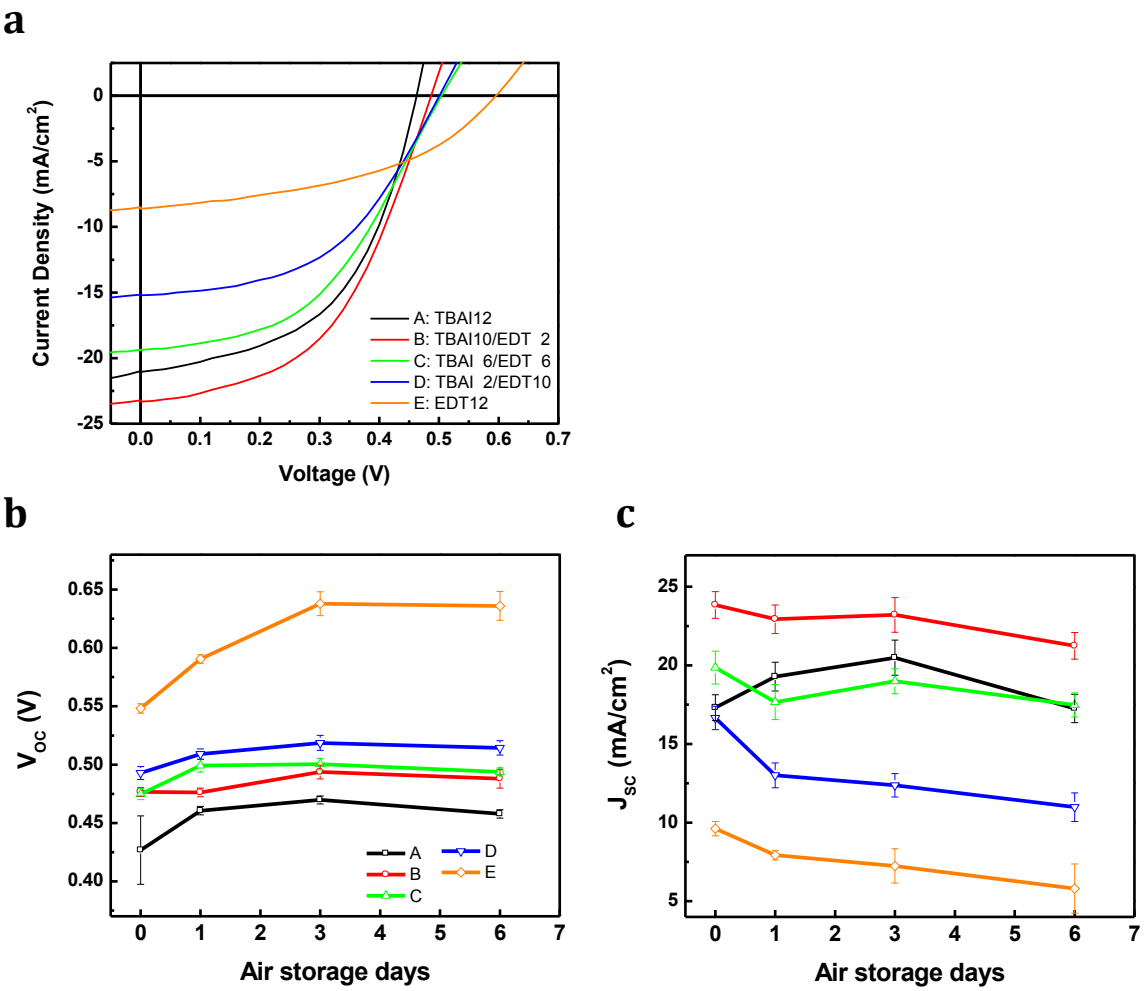

Figure S3 | Comparison of devices with different numbers of PbS-TBAI and PbS-EDT layers. **a,** Representative J-V curves. **b,** and **c,** The change of V_{OC} and J_{SC} with air storage time, respectively. The device structure is ITO/ZnO/PbS-TBAI(x)/PbS-EDT(y)/MoO_3/Al, where x and y denote the numbers of PbS-TBAI and PbS-EDT layers. The total number of PbS layers is 12 layers in all devices. The PbS-EDT-only device (Device E) exhibits the lowest J_{SC} but highest V_{OC} among all devices. It also shows a decreasing J_{SC}, and an increasing V_{OC} with air-exposure time. By replacing the top 2 PbS-TBAI layers with PbS-EDT layers (Device B), the J_{SC} significantly increased compared to the PbS-TBAI-only device (Device A). We conclude that the PbS-TBAI layer is the main absorber layer and the improvement in J_{SC} in PbS-TBAI/PbS-EDT devices shown in Fig 1b is not from additional light absorption from the PbS-EDT layer. This can be further supported by the progressively decreasing J_{SC} with decreasing numbers of TBAI layers in devices B to D.

Ultraviolet Photoelectron Spectroscopy (UPS)

UPS is used to determine the Fermi level (E_F) and the valence band maximum (E_V) with respect to vacuum level (E_{VAC}) of the PbS thin films. The basic principles and an example spectrum are shown in Fig. S4.

For a photoelectron to escape the sample surface and to be collected, it has to have sufficient energy to overcome the sum of the binding energy (with respect to E_F) of its initial level and the work function (Φ), where $\Phi = E_{VAC} - E_F$. Therefore, for a fixed incident photon energy of 21.2 eV, the secondary electron cut-off (high binding energy edge) represents photoelectrons with zero kinetic energy (E_k) when they escape the sample surface and their initial level is shown as the grey dotted line inside the DOS in Fig. S4a. The work function Φ is determined by the difference between the incident photon energy (21.2 eV) and the binding energy of the secondary electron cut-off. In the example spectrum (Fig. S4b), the cut-off binding energy is 16.43 eV as determined by the intersection of the linear portion of the spectrum and the baseline. The work function of this sample is thus Φ=21.2-16.43=4.77 eV; that is, E_F is -4.77 eV with respect to E_{VAC}. The difference between E_F and E_V is determined by the intersection of the linear portion of the spectra near the Fermi edge (low binding energy region) with the baseline. The example spectrum has a E_F - E_V=0.82 eV. Therefore, its valence band maximum E_V is -5.59 eV with respect to E_{VAC}. The conduction band minimum (E_C) is further calculated by adding the optical bandgap, as determined by the position of the lowest exciton absorption peak, to E_V.

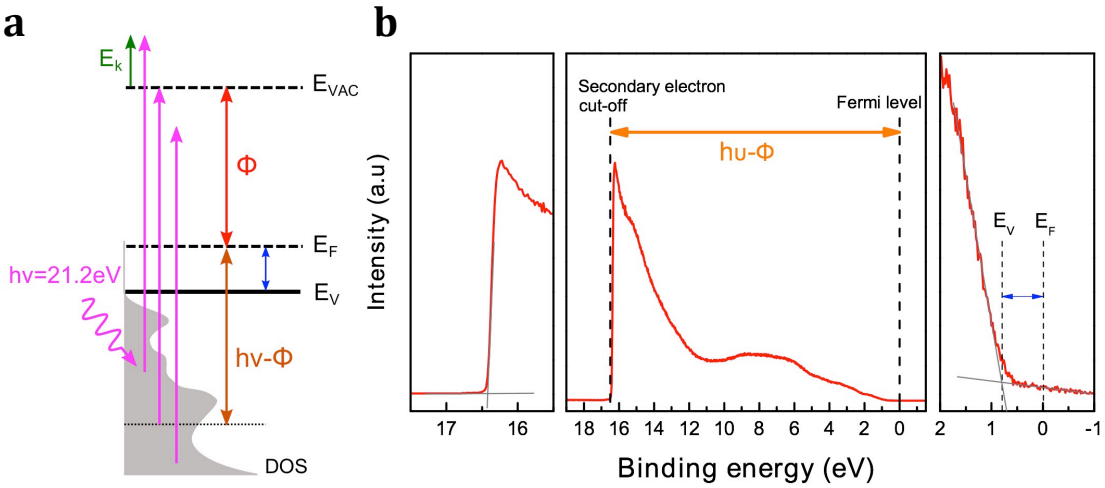

Figure S4 | Basic principles of UPS measurements. a, Schematic illustration of the energy diagram. DOS: density of states in the valence band. **b,** An example UPS spectrum. The left panel shows the magnified view of the high binding energy region and the right panel shows the magnified view of the low binding energy region. Grey lines represent the linear fits.

Band alignment between PbS-TBAI and PbS-EDT

Thickness-dependent UPS is used to determine the band alignment between PbS-TBAI and PbS-EDT. The thickness of the thickest PbS-EDT overlayer corresponds to the thickness generally used in devices and is determined to be ~45nm by a profilometer. This thickest PbS-EDT layer was obtained in the same manner as for device fabrication (2 layer-by-layer spin-coating steps from 50 mg/ml PbS solution followed by ligand exchange with EDT solution). The thinner PbS-EDT layers (4.5 nm, 9 nm, 13.5 nm) were obtained by spin-coating dilute PbS solution (10 mg/ml) on PbS-TBAI. The thicknesses of these thinner PbS-EDT layers were estimated by the solution concentration (10 mg/mL, 5 times less than for the thickest layer) and the numbers of layer-by-layer spin-coating steps (1, 2, and 3 steps, respectively).

As shown in Fig. S5, two distinct peaks from PbS-EDT (~3.8eV and ~5.8eV) appear in the UPS spectra after we add PbS-EDT on PbS-TBAI. The secondary electron cut-off shifts to higher binding energy while the E_F - E_V decreases with increasing thickness of PbS-EDT. These features indicate interfacial band bending at the PbS-TBAI/PbS-EDT interface. The fitted band positions are plotted in Figure 2a and summarized in Table S1. We note that the saturation of the spectral shape and the band positions at ~13.5nm also confirms that the ~45nm of PbS-EDT layer used in our photovoltaic devices is thick enough to result in a continuous overlayer and its thickness may be beyond the width of the interfacial band bending region.

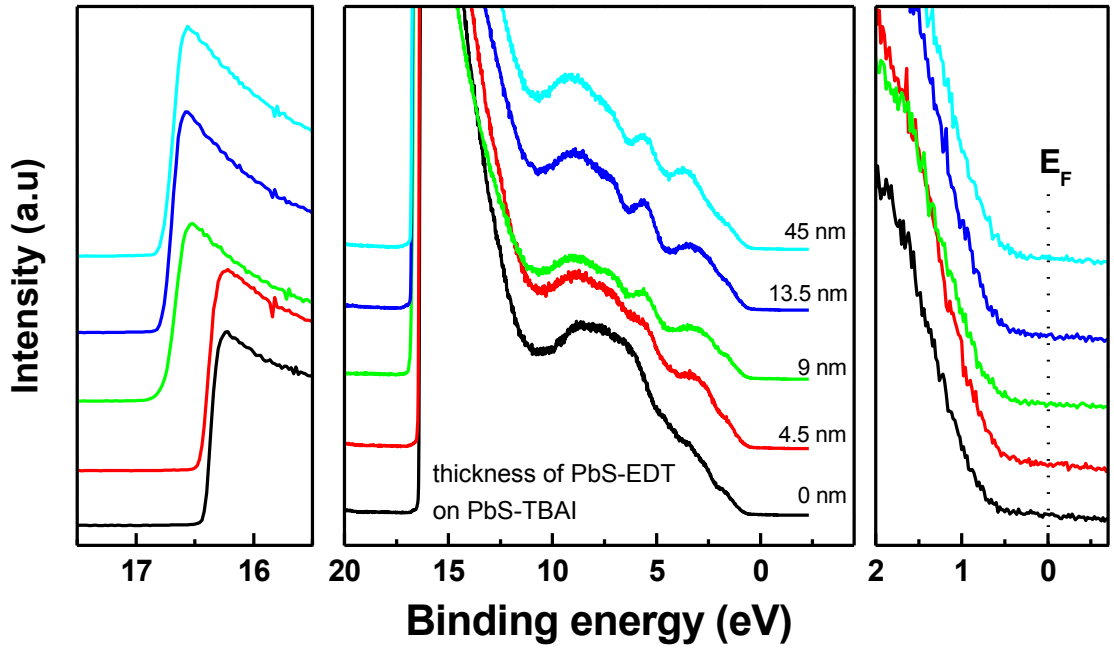

Figure S5 | UPS spectra of PbS-TBAI films covered with different thicknesses of PbS-EDT. The left panel shows the secondary electron cut-off region and the right panel shows the magnified spectra near Fermi edge. Spectra were shifted for clarity.

Table S1. Band positions with respect to vacuum as determined from the UPS spectra in Fig S5. The error bars in E_F-E_V represent the error from fitting.

Sample	E_C	E_F	E_V	E_F-E_V
TBAI (110nm)	-4.26	-4.77	-5.59	0.82±0.02
TBAI (110nm)/ EDT (4.5nm)	-4.10	-4.73	-5.46	0.70±0.02
TBAI (110nm)/ EDT (9.0nm)	-3.78	-4.41	-5.11	0.70±0.02
TBAI (110nm)/ EDT (13.5nm)	-3.68	-4.38	-5.01	0.63±0.02
TBAI (110nm)/ EDT (45.0nm)	-3.68	-4.38	-5.01	0.63±0.02

The thickness-dependent UPS data allow us to determine interfacial band bending at the PbS-TBAI/PbS-EDT interface. At equilibrium, the Fermi level in the whole sample must align. Therefore, the relative band alignment can be determined by matching the Fermi level and then placing the band edge energies with respect to the Fermi level. It can be better understood with the help of the schematic illustrations shown in Figure S6. The left figure shows the experimentally determined band positions with respect to vacuum level as a function of the thickness (d_n) of PbS-EDT on PbS-TBAI. The reduction of work function after adding the PbS-EDT layer implies a downward vacuum level shift, whereas the reduction of E_F - E_V implies an upward band bending from the interface to PbS-EDT. Once the thickness of the PbS-EDT is greater than the width of the interfacial band bending region, the band positions and the UPS spectra reach saturation (d_2 and d_3). The right figure shows the band alignment deduced from the left figure.

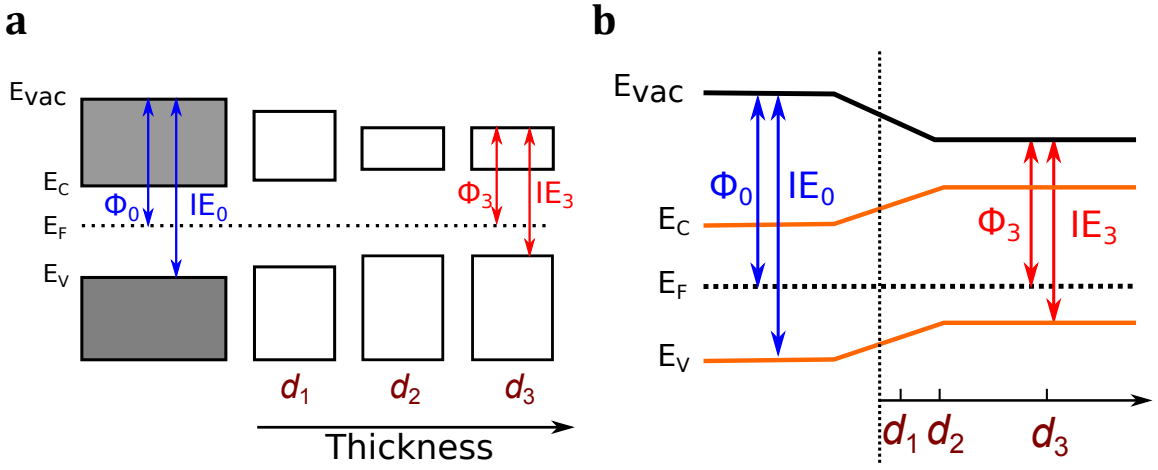

Figure S6 | Schematic illustrations explaining how to determine the band alignment at the interface from the UPS spectra. a, The band positions as a function of the overlayer thickness (d_n). Here, the conduction band edge (E_C), valence band edge (E_V) and vacuum levels (E_{VAC}) are referenced to the Fermi level (E_F). IE: ionization energy. **b**, The corresponding band alignment. For simplicity, the conduction band and valence band are connected by straight lines.

As a control experiment, we compare the UPS data of PbS-TBAI film and PbS-TBAI film soaked in EDT solution (Fig. S7). Soaking the PbS-TBAI film in EDT solution without depositing a new PbS-EDT layer does not change the work function significantly but slightly decreases the valence band offset (E_F-E_V) from 0.82 eV to 0.75 eV. Therefore, simply soaking the PbS-TBAI film in EDT solution is not enough to give rise to a significant conduction band offset (valence band offset) that can block electron flow (facilitate hole extraction). Furthermore, the features from PbS-EDT (~3.8 eV and 5.8 eV) do not appear in the EDT-soaked PbS-TBAI film, suggesting that soaking PbS-TBAI films in EDT solution cannot change it into PbS-EDT.

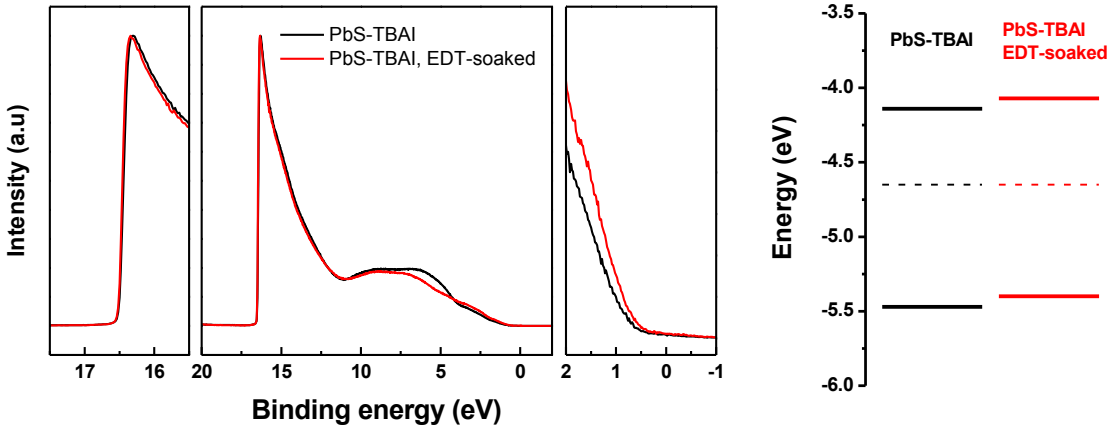

Figure S7 | UPS spectra of a PbS-TBAI film and a PbS-TBAI film soaked in EDT solution without depositing a new PbS-EDT layer. The right figure shows the corresponding band positions with respect to vacuum.

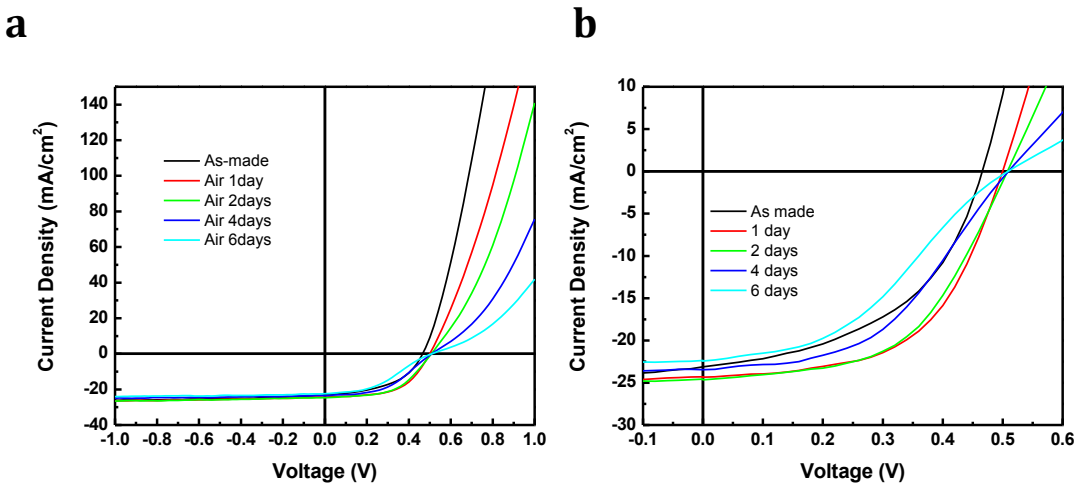

Figure S8 | Development of S-shape J-V characteristics in a PbS-TBAI/PbS-EDT device with MoO_3/Au anode after air-exposure. b shows the magnified view of **a**.

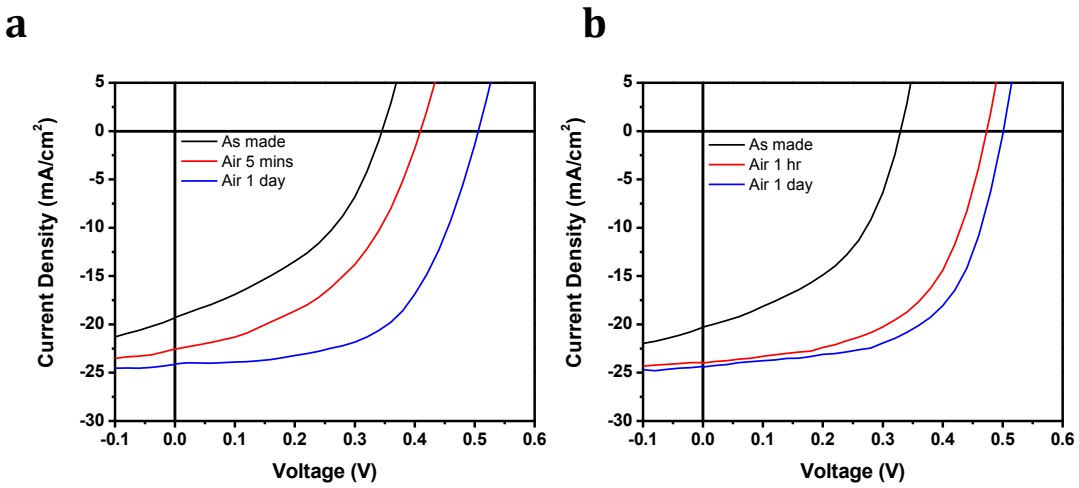

Figure S9 | Examples of initial increase of device performance after short air-exposure time after evaporation of the metal electrodes. The device structure is ITO/ZnO/PbS-TBAI/PbS-EDT/Au. **a** and **b** were fabricated in the same conditions but on different substrates. The devices were fabricated and stored in air overnight before anode deposition under vacuum. The air-exposure time shown here represents further air-exposure time after anode evaporation under vacuum.

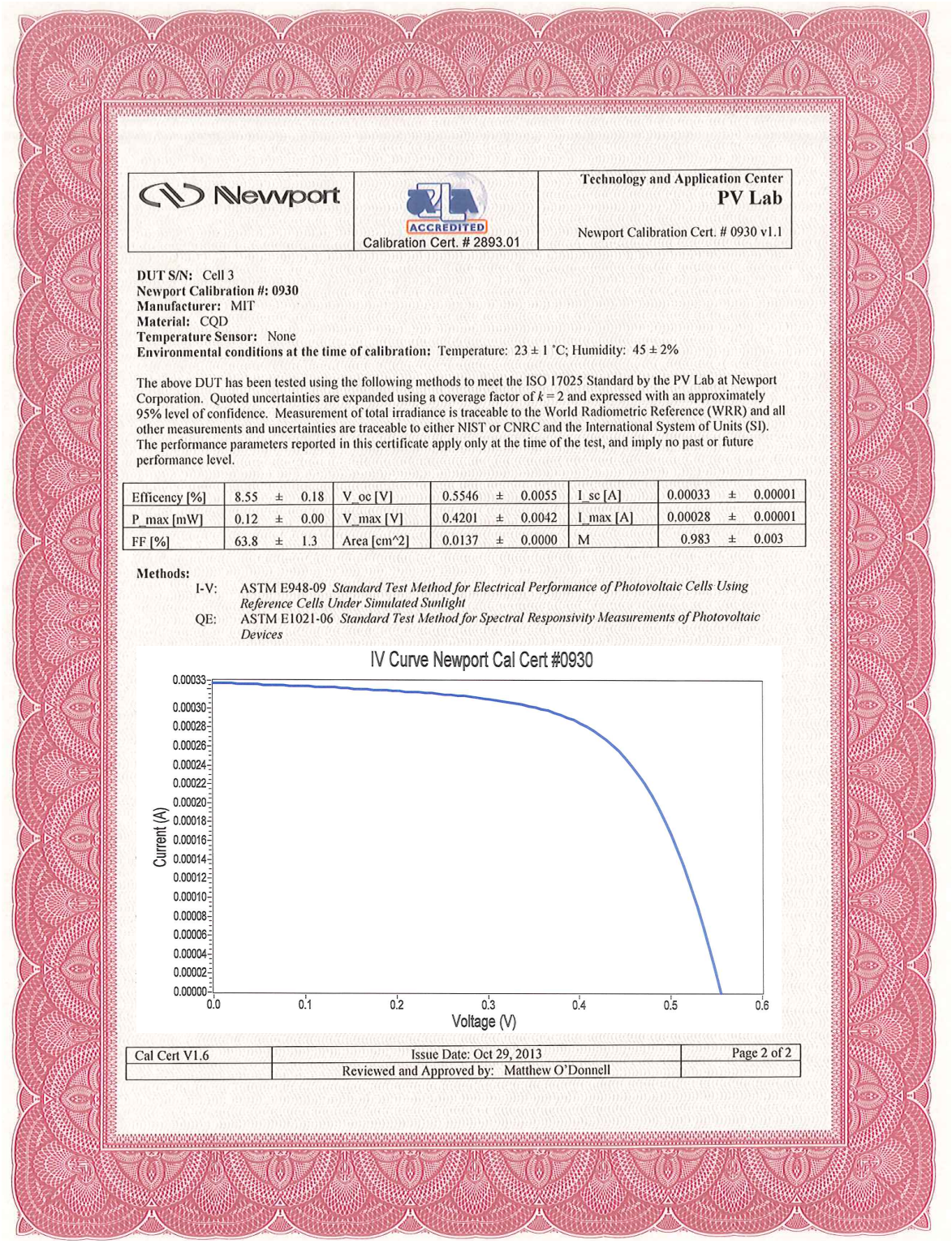

Newport

ACCREDITED
Calibration Cert. # 2893.01

Technology and Application Center
PV Lab
Newport Calibration Cert. # 0930 v1.1

DUT S/N: Cell 3
Newport Calibration #: 0930
Manufacturer: MIT
Material: CQD
Temperature Sensor: None
Environmental conditions at the time of calibration: Temperature: 23 ± 1 °C; Humidity: 45 ± 2%

The above DUT has been tested using the following methods to meet the ISO 17025 Standard by the PV Lab at Newport Corporation. Quoted uncertainties are expanded using a coverage factor of $k = 2$ and expressed with an approximately 95% level of confidence. Measurement of total irradiance is traceable to the World Radiometric Reference (WRR) and all other measurements and uncertainties are traceable to either NIST or CNRC and the International System of Units (SI). The performance parameters reported in this certificate apply only at the time of the test, and imply no past or future performance level.

Efficency [%]	8.55	±	0.18	V_oc [V]	0.5546	±	0.0055	I_sc [A]	0.00033	±	0.00001
P_max [mW]	0.12	±	0.00	V_max [V]	0.4201	±	0.0042	I_max [A]	0.00028	±	0.00001
FF [%]	63.8	±	1.3	Area [cm^2]	0.0137	±	0.0000	M	0.983	±	0.003

Methods:

I-V: ASTM E948-09 *Standard Test Method for Electrical Performance of Photovoltaic Cells Using Reference Cells Under Simulated Sunlight*

QE: ASTM E1021-06 *Standard Test Method for Spectral Responsivity Measurements of Photovoltaic Devices*

Cal Cert V1.6	Issue Date: Oct 29, 2013	Page 2 of 2
	Reviewed and Approved by: Matthew O'Donnell	

Figure S10 | Certified record efficiency to date for colloidal quantum dot solar cells. This unencapsulated device had been stored in air for 37 days before being tested in air by an accredited laboratory.

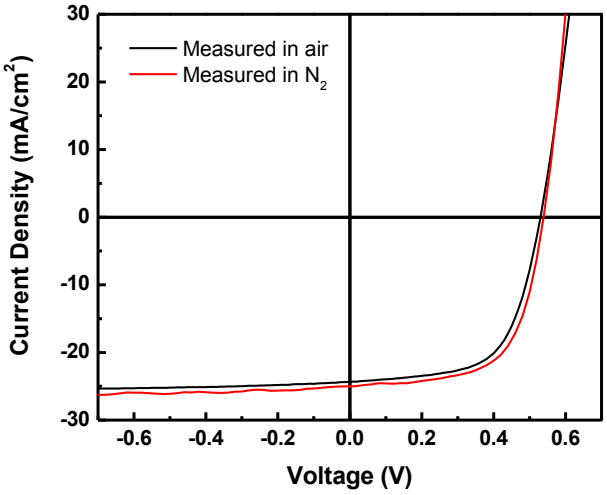

Figure S11 | J-V characteristics of an unencapsulated PbS-TBAI/PbS-EDT device with Au anode measured in air and under inert N_2-atmosphere. No significant difference in performance was found when the device was measured in air. The slight difference is attributed to the different solar simulators used for each measurement and other experimental uncertainties.

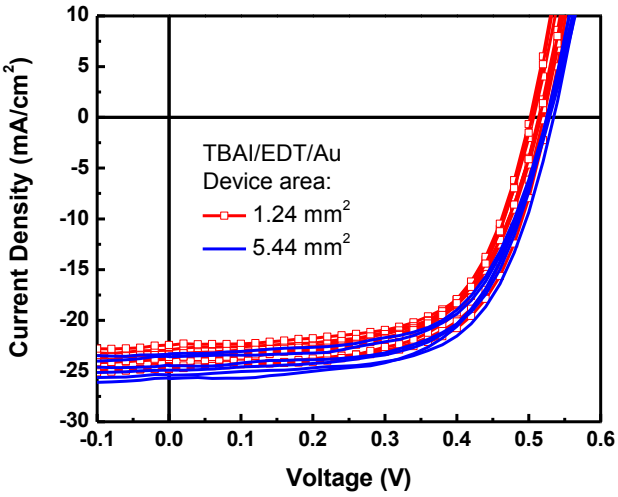

Figure S12| J-V characteristics of devices with different device areas. To test the scalability and reduce the experimental error in determining device area, we fabricated devices with a device area of 5.44 mm^2, ~4 times larger than our typical devices (1.24 mm^2). The figure plots the J-V curves of nine devices with 1.24 mm^2 and six devices with 5.44 mm^2 area. Devices with a larger device area show similar performance.

Newport

ACCREDITED
Calibration Cert. # 2893.01

Technology and Application Center
PV Lab
Newport Calibration Cert. # 0972

DUT S/N: Cell A
Newport Calibration #: 0972
Manufacturer: MIT
Material: CQD
Temperature Sensor: None
Environmental conditions at the time of calibration: Temperature: 23 ± 1 °C; Humidity: 45 ± 2%

The above DUT has been tested using the following methods to meet the ISO 17025 Standard by the PV Lab at Newport Corporation. Quoted uncertainties are expanded using a coverage factor of $k = 2$ and expressed with an approximately 95% level of confidence. Measurement of total irradiance is traceable to the World Radiometric Reference (WRR) and all other measurements and uncertainties are traceable to either NIST or CNRC and the International System of Units (SI). The performance parameters reported in this certificate apply only at the time of the test, and imply no past or future performance level.

Efficency [%]	8.19	±	0.17	V_oc [V]	0.5518	±	0.0055	I_sc [A]	0.00066	±	0.00001
P_max [mW]	0.24	±	0.01	V_max [V]	0.4300	±	0.0043	I_max [A]	0.00057	±	0.00001
FF [%]	66.7	±	1.4	Area [cm^2]	0.0298	±	0.0001	M	1.037	±	0.007

Methods:

I-V: ASTM E948-09 *Standard Test Method for Electrical Performance of Photovoltaic Cells Using Reference Cells Under Simulated Sunlight*

QE: ASTM E1021-06 *Standard Test Method for Spectral Responsivity Measurements of Photovoltaic Devices*

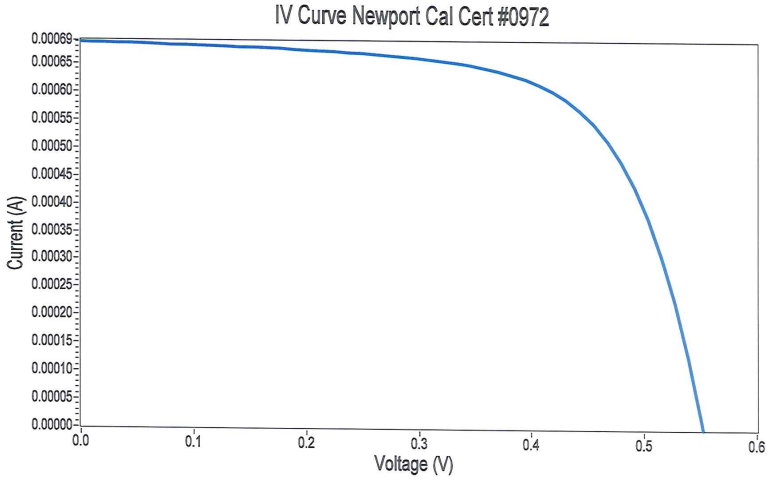

Cal Cert V1.6	Issue Date: Feb 19, 2014	Page 2 of 2
	Reviewed and Approved by: Matthew O'Donnell	

Figure S13 | Certified performance for a high fill factor device with larger area. This device was certified after 131 days of air storage and showed the highest fill factor of 66.7% in QD solar cells to date. The nominal total device area for this device is 5.44 mm^2 as defined by the overlap of the anode and cathode. For the certification, a 3 mm^2 mask was attached to the device to define the device area.

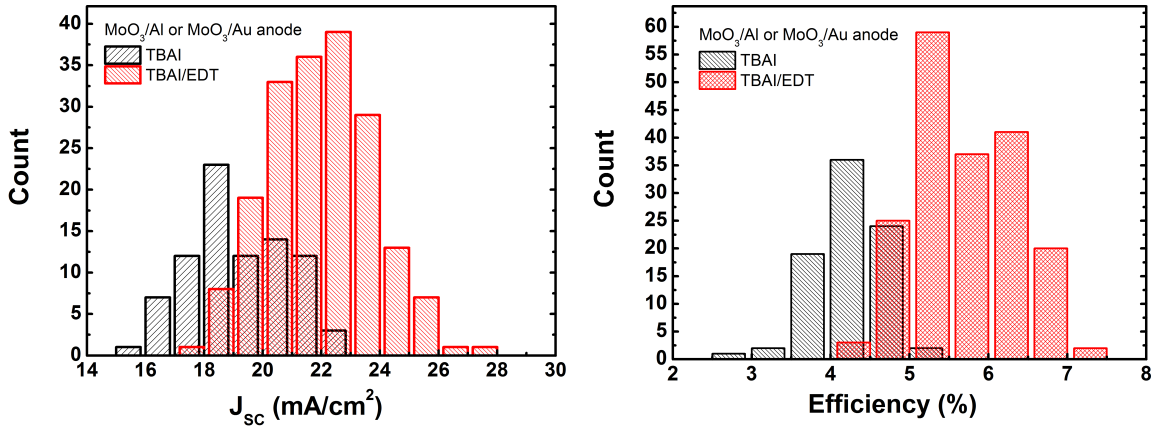

Figure S14 | Histograms of J_{SC} and power conversion efficiency of devices with MoO_3 anodes. The histograms show the performance of devices on different substrates from different batches using the same size of PbS QDs. The PbS-TBAI/PbS-EDT devices consistently outperform the PbS-TBAI devices in every batch of devices we fabricated.

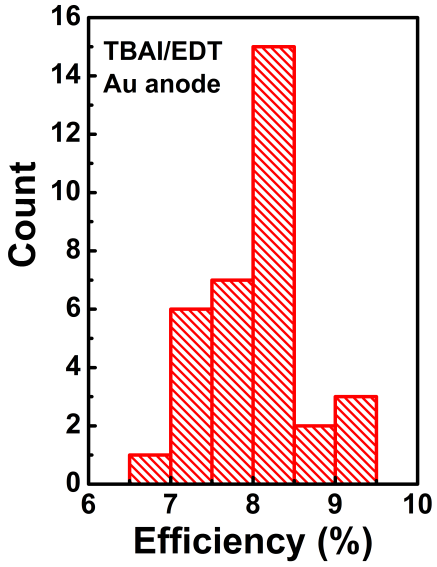

Figure S15 | Histograms of power conversion efficiency of PbS-TBAI/PbS-EDT devices with Au anodes. The histogram shows the efficiency of more than 30 devices with Au anodes on different substrates. Unlike the devices with MoO_3 anodes whose air-stability vary due to the uncontrolled ambient humidity, all of the devices with Au anode exhibit excellent air stability.

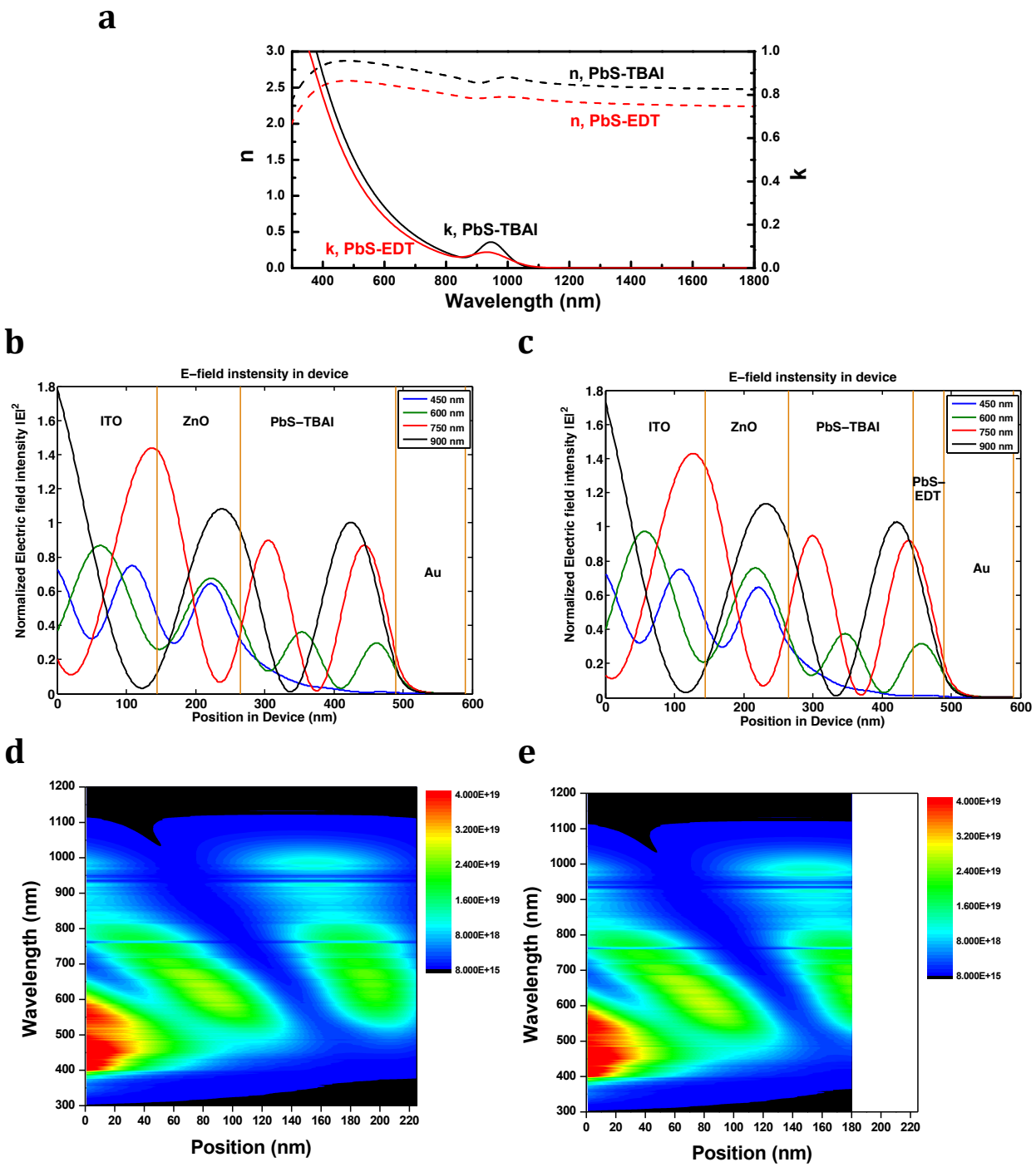

Figure S16 | Optical modeling results. a, the complex refractive indices of PbS-TBAI and PbS-EDT films as determined by ellipsometry. **b** and **c**, modeled electric filed intensity in the devices for four selected wavelengths. **d** and **e,** modeled photon absorption rate (1/sec-cm^3) in the PbS-TBAI main absorbing layer under 1-sun AM1.5G illumination. **b** and **d**, PbS-TBAI-only device; **c** and **e**, PbS-TBAI/PbS-EDT device. The position at 0 nm represents the ZnO/PbS-TBAI junction. The horizontal stripes are due to the dips in the AM1.5G solar spectrum (O_2 and H_2O absorption). The results show that the optical field is similar in PbS-TBAI-only and PbS-TBAI/PbS-EDT devices. No new optical modes developed in the PbS-TBAI/PbS-EDT devices. Moreover, a significant portion of the longer wavelength photons (>500nm) is absorbed deeper in the film, i.e. close to the PbS-TBAI/PbS-EDT interface. Optical modeling was performed by using a model and codes from literature[S1].

Reference

S1. Burkhard, G. F., Hoke, E. T. & McGehee, M.D. Accounting for interference, scattering, and electrode absorption to make accurate internal quantum efficiency measurements in organic and other thin solar cells. *Adv. Mater.* **22**, 3293 (2010) ;
code: http://www.stanford.edu/group/mcgehee/transfermatrix/index.html.